DINAME 2019 - Proceedings of the XV International Symposium on Dynamic Problems of Mechanics,
M.A. Savi, T.G. Ritto and W.M. Bessa (Editors), ABCM, Buzios, RJ, Brazil, March 10th to 15th, 2019

An Integrated Design Method for Membrane-Type Acoustic Metamaterials

Sampaio, Lucas Yudi Moriya [1], de Oliveira, Leopoldo Pisanelli Rodrigues [1]

[1] Escola de Engenharia de São Carlos, Universidade de São Paulo, Av. Trabalhador São-Carlense, 400, 13565-090 São Carlos – SP, Brasil, yudimoriya@gmail.com.

Abstract: Membrane-type acoustic metamaterials recently emerged as a reliable, compact and lightweight solution to acoustically impaired environments. With their unusual properties of negative mass and bulk modulus, a transmission loss performance superior to the one predicted by the mass-density law is feasible, asserting their certain role in modern acoustics. Since the first membrane acoustic metamaterial was proposed, several new concepts arose in the scientific community in order to improve its performance in terms of sound transmission loss level and bandgap extension. These concepts, although constructively different, contain in essence the three fundamental elements that characterize membrane acoustic metamaterials: a mass-, a stiffness- and a boundary-element. The combination of these elements defines a metamaterial's cell, which can present different resonant properties according to the dynamic behavior of each component. The present research has explored this modular construction to propose an integrated design method for metamaterial design, analyzing the resonant behavior of possible elements in order to propose new metamaterial concepts. Fully coupled vibro-acoustic simulations were used to model these elements and to analyze the resulting sound transmission loss profile of a novel metamaterial concept and were compared by results obtained in an impedance tube. Three different concepts were analyzed: a sole membrane, a decorated membrane resonator and a Helmholtz resonator coupled with the latter. It was seen that the concepts exhibited improvement relative to the acoustic mass-law in different levels and bands. The Helmholtz resonator coupled cell did present the particular resonances of its elements and thus the best performance, which also validated the proposed design method.

Keywords: metamaterials, acoustics, membrane, transmission loss, modelling

INTRODUCTION

As modern engineering focus in the design of lightweight, reliable systems, it spends most of its effort ensuring an optimal structural performance and stability. Despite these advancements, acoustic design remains often unsatisfactory, since conventional materials are bound to the mass-density law transmission behaviour (London, 1949), which implies that a lightweight approach would actually worsen an envisioned noise control. In another scenario, where low-frequency sound absorption is desired, the traditional porous absorber technique is either insufficient or too cumbersome for a practical solution. Both situations are common issues of acoustic treatment and could be solved by the current state of the art in acoustics research: acoustic metamaterials.

The field of acoustic metamaterials has grown drastically in the past twenty years as an extension of the optic's photonic crystal research (Klironomos and Economou, 1998; Kushwaha et al., 1993), since acoustic waves exhibited the same distinct behaviour as observed in its electromagnetic counterpart. These unusual properties were initially attributed to Bragg's scattering and later on to local resonances in the material's structure, which are perceived through negative effective mass density (medium moves in opposite direction of force) and/or bulk modulus (medium expands upon compression) in an specific bandwidth (Cummer, Christensen and Alù, 2016). As a result, some locally resonant metamaterials exhibit in this frequency range exceptional subwavelength wave reflection and absorption and can induce phenomena such as wave non-reciprocity (Fleury et al., 2015) and cloaking (Cummer and Schurig, 2007). Though many of these developments are still only affordable under laboratory conditions, metamaterial research has also concerned itself with more practical acoustic treatment solutions, which can simultaneously attend to modern design requisites and surpass the performance of current designs. Membrane-type acoustic metamaterials (MAMs) are the clear example of this effort due to their high sound transmission loss (STL) potential allied with a simple, small-sized and lightweight construction.

The concept of MAMs derived from the first realization of locally resonant acoustic metamaterials (Liu et al., 2000), being conceived as a bi-dimensional approach to the original proposal. Yang et al. (2008) envisioned a decorated membrane resonator (DMR), composed of a mass, a stiffness and a boundary element, represented in this case by a hard disk attached to a pre-stressed elastic membrane fixed on a rigid grid, respectively. This combination acting as a sound barrier to a plane wave revealed a STL behaviour containing two dips associated with the DMR's resonance frequencies and a reflection associated peak right after the first resonance. This STL maximum in a low frequency band is superior to the STL predicted by the mass-density law, thus characterizing the DMR as a locally resonant acoustic metamaterial and fomenting further development from the concept. The desired improvements included mainly a bandgap extension for

broadband noise insulation, an absorption-focused approach to the original DMR and the ability to actively manipulate MAMs for adaptive applications.

DESIGN ELEMENTS OF A MAM CELL

After a decade of MAM development since the first DMR, many new concepts arose to attend the mentioned goals, but still conformed to the cited mass-, stiffness- and boundary-element categorization. As each part contributes significantly to the resulting acoustic performance, the idea of modularity seems natural to MAMs. In modular product development (MPD), modular products refer to assemblies that fulfil various functions through the combination of different building blocks (Huang, 2000), which in MAMs is applicable in two levels: first, the balance between mass- and stiffness-element and their coupling with the boundary-element; and second, the coupling between distinct MAM cells panel- and/or layer-wise. In both stages, a standardized workflow of its conception is desired, in order to properly balance each element's role in the end product. An integrated design method is thus of great interest for such constructions, and is sought in this work.

First, a thorough description of each module is envisioned to comprehend the categorization of the existent designs and their respective physical principles and functionalities. The present manuscript focusses, in particular, on the first stage design of MAMs, leaving the interaction between multiple cells to future work. The mentioned elements of are represented in Fig. 1. Then, a case study is presented to illustrate the validity of an integrated design approach to these metastructures.

Figure 1 – Proposed elements of a MAM cell

Stiffness-Element

The foundation of MAM's extraordinary performance lies unexpectedly in the application of thin elastic membranes as its stiffness element. Conventional sound insulating materials follow the transmission behavior described by the equation:

$$\mathbf{STL} = \mathbf{10} \cdot \mathbf{log}\left(\frac{\boldsymbol{\rho_s \omega}}{\mathbf{2\rho c}}\right)^{\mathbf{2}} \tag{1}$$

The 'mass law' presented in Eq. (1), valid for frequencies below the *coincidence effect* and normal incident waves, indicates that STL increases at 6 dB per doubling of frequency ω [rad/s] and per doubling of superficial mass density ρ_s [kg/m²] (Möser, 2015). Thus, it becomes clear that low frequency sound attenuation is compromised in small, lightweight barriers, and how to solve it using elastic materials with submillimetre thickness would be counterintuitive. Nevertheless, such materials contain very weak elastic moduli, which is precisely why low frequency oscillation patterns appear even in small boundary-limited samples (Yang et al., 2008). These patterns correspond to vibration modes that induce transgressions of the *mass law*, which allow improvement of STL in low frequency regime near their respective resonant frequencies.

Transmission peaks and dips appear in the frequency response of these local resonant units because of the membrane's dynamic behavior. Considering an acoustically excited sample, its displacement can be decomposed as $\vec{u} = \Delta\vec{u} + \langle u_z \rangle$, where $\langle u_z \rangle$ represents the surface-averaged normal displacement of the membrane and $\Delta\vec{u}$ the remaining oscillatory motion. The air layer next to it must satisfy the dispersion relation:

$$\mathbf{k}_{\parallel}{}^{2} + \mathbf{k}_{\perp}{}^{2} = \left(\frac{\mathbf{2\pi}}{\boldsymbol{\lambda}}\right)^{\mathbf{2}} \tag{2}$$

where $k_{\parallel(\perp)}$[1/m] represents the parallel (perpendicular) wavenumber vector. For $\langle u_z \rangle$, $k_{\parallel}$ peaks at zero, relating this displacement to a radiation-coupled "pistonlike" motion whose transmitted field has the same wave vector $k_{\perp}$ and accounts for far-field sound. As for $\Delta\vec{u}$, since the sample size has an order of a few centimeters and low frequency sound is considered, $k_{\parallel}$ is necessarily greater than $2\pi/2R > 2\pi/2\lambda_{low\ freq}$. This leads to $k_{\perp}^2 < 0$, which characterizes evanescent, non-radiating modes associated to near-field transmission. Thus, when $\langle u_z \rangle = 0$, despite of remaining oscillations, total reflection occurs, leading to a transmission dip (Yang et al., 2008;Yang et al., 2013).

With a better understanding of the dynamics behind STL in elastic surfaces, the question of tuning these radiating and non-radiating modes becomes important. The relationship between the mechanical properties of an elastic surface and its acoustic influence can be approached by means of numerical/analytical modelling. Although membranes were traditionally modelled as tension-dependent materials, opposed by flexural rigidity-dependent plates (Zhang et al., 2012), vibration of any structure is a product of both parameters, resulting in the following modal equation (Blevins, Lau and Wang, 2016):

$$\mathbf{D\nabla^4 w + T\nabla^2 w = -\rho_s \frac{\partial^2 w}{\partial t^2}} \tag{3}$$

where $\mathbf{D = \frac{Eh^3}{12(1-\upsilon^2)}}$ represents the bending stiffness and T [N/m] the applied tension. These three parameters have influence in the mode's corresponding resonant frequencies and can be chosen accordingly. In dynamics, the following matrix relation provides the natural frequencies of a system:

$$\boldsymbol{\omega^2 = \frac{K}{M}} \tag{4}$$

where K represents the stiffness matrix, whereas M is called the mass matrix. Both D and T contribute to the stiffness part, being then directly proportional to the squared resonant frequencies. Concerning D, it was previously thought that a low elastic modulus E was necessary for a short decay length of the mentioned evanescent waves, but Naify et al. (2010) used elastic materials with E several orders of magnitude greater than the thought threshold and obtained similar results. The flexural rigidity plays a lesser role in K, thus affecting ω with less sensitivity, whilst tension plays a major role in altering not only ω but the STL amplitude proportionally (Zhang et al., 2012). Similarly, ρ_s contributes to M being inversely proportional to ω^2, shifting the modes to lower frequencies with higher mass.

Geometrical parameters such as membrane size and shape are also of influence. By reducing cell size and/or increasing thickness, a shift of the transmission peak to higher frequencies is expected, extending the bandwidth of the high STL region (Sui et al., 2015). As to shapes, although history presented mostly squares and circles, different ones can be used to the same effect (Yang et al., 2008). Since the vibration mode's shape is dependent of the membrane's geometry, some alteration in which mode induces a transmission peak or dip is possible, but still conform to the $\langle u_z \rangle$ associated with the mode.

Mass-Element

Although no-mass-attached membranes are potentially lighter and can introduce high STL at low frequencies, constructions with an attached mass have been predominant in MAM research (Sui et al., 2015). The reason behind such trend is the possibility of enhancing low frequency performance with more controllability and independence from elastic properties of the stiffness-element. As highly elastic materials often exhibit non-linear behavior and tend to gain density with stiffness, the addition of a coupled element that commands the mass portion of Eq. (4) helps not only in achieving lower resonant frequencies but also in manufacturing and tunability of the MAM. The single drawback, besides weight increment, lies in the narrowband STL peak, which in higher frequencies tends to result in a worse STL compared to an equivalent massless membrane.

The fundamental mass-element has been present since the first locally resonant metamaterial in (Liu et al., 2000), in the form of a centered single concentrated mass. In MAMs, it took form of a rigid disk of known mass, composing the DMR observed in (Yang et al., 2008) and subsequent works, which displays the radiating vibration modes seen in Fig. (2), obtained from finite element model (FEM) simulations.

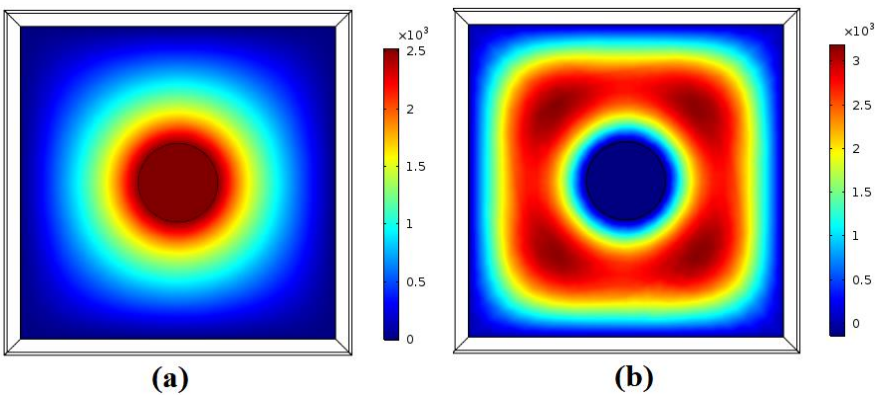

Figure 2 – Normal displacement from radiating modes of a DMR obtained in FEM simulation

In both modes, a transmission peak is present due to a non zero $\langle u_z \rangle$. An anti-resonance exists between modes (a) and (b), corresponding to a superposition of their amplitudes in opposite phase and containing the amplitude maxima of the

two, leading to $\langle u_z \rangle = 0$ (Naify et al., 2010; Yang et al., 2008). The resulting transmission dip tends to follow the first peak, whilst remaining almost immune to changes of the second peak. Mode (a) corresponds to the first mode of any vibrating surface whose maximum displacement is centered. In this case, it is accentuated by the rigid mass, which contributes to amplify the first transmission peak and dip, as well as shift them to lower frequencies. Contrarily, mode (b) presents a node in the centered region and maximum displacement between it and the cell's boundary, thus being practically only membrane-dependent. The first mode and anti-resonance are then described as mass-dominated, being subject to the added mass density and tension, whereas the second mode is membrane-dominated, being dependent of the elastic material's superficial density and tension (Zhang et al., 2012).

Due to the coincident position of mass and mode (a)'s amplitude maximum, the original DMR configuration boosts this mode's influence resulting in a narrowband low-frequency STL, which is solely inapplicable in most situations since noise sources are rarely tonal. Different mass-element related approaches have been researched in order to extend the usable STL bandwidth and compose the possible arrangements for the present module.

Perhaps the simplest alteration of the original concept was moving the mass-element to an eccentric location, altering the previous mode shapes and adding another radiating mode with an associated anti-resonance. Zhang et al. (2012) moved the concentrated mass laterally and diagonally and analyzed how the first resonance and STL peak shifted in frequency. Chen et al. (2014) reports that the first mode acquires strong rotational motion allied with the former translation, the second consists primarily in rotation of the mass and the third accounts for the membrane's vibration with flapping movement of the mass. The last mode is the most sensitive to eccentricity and shifts significantly to lower frequencies with more eccentric mass locations, whereas the first and second modes tend to shift to higher frequencies with less magnitude.

Aside from a dislocated center-of-mass, multiple masses are also commonly employed as concept for altering the membrane's vibration modes. Naify et al. (2011) demonstrates the potential of using multiple coaxial ring mass-elements in MAMs in extending the STL over frequency. They concluded that the mass-dominated resonance tends to shift upward in frequency when mass was concentrated away from center, agreeing with what was proposed for eccentric masses. Additionally, attaching multiple rings resulted in new radiating vibration modes and new STL peaks and dips. Their corresponding resonant frequencies depend highly of the mass distribution of the rings, which if uniform promotes a multi-peak STL and if non-uniform results in a broadband STL peak due to an approach of both mass-dependent modes in frequency. An application of ring mass-elements appears in (Langfeldt et al., 2017), where the ring mass, associated with a perforated membrane, forms an air neck similar to Helmholtz resonators and introduces another resonance prior to the membranes first mode, adding a STL peak thoroughly dependent of the ring and perforation characteristics.

A combination of eccentricity and multiple asymmetric masses has led to the development of so called "dark" acoustic metamaterials by Mei et al. (2012), which present extraordinary sound absorption, instead of reflection, during resonance. These MAMs consist of rectangular membranes and semi-circular masses equally distanced from center backed by an aluminum reflector. The principle of sound absorption lies in the conversion of acoustic to elastic energy through the flapping movement of the masses, already mentioned to be present in eccentric cases, followed by efficient dissipation. Vibrating modes related to the flapping movement of masses ar shown in Fig. 3. Influent parameters are the mass of the elements for the first absorption peak and the distance between them for the second (Huang, Shen and Jing, 2016). Such MAMs are also analytically modelled in (Chen et al., 2014) and applied laterally in waveguides in (Fu et al., 2017).

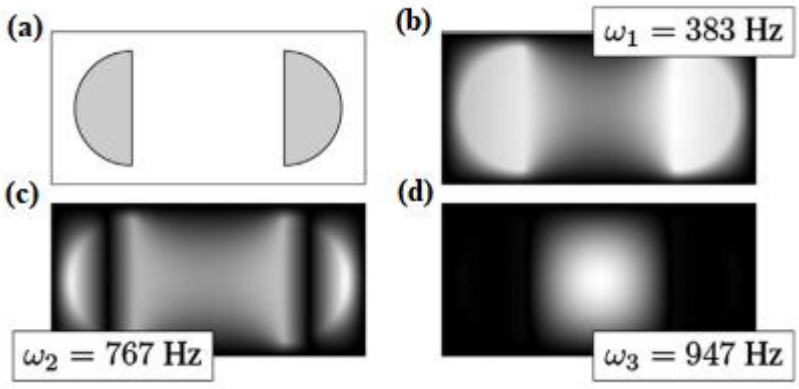

Figure 3 – Front view of a "dark" acoustic metamaterial (a) and normal displacement of its vibrating modes below 1000 Hz (b-d). Source: Yang et al. (2015)

Although mass-elements have mostly taken circular-related shapes due to simpler construction, arbitrary shapes can be modelled according to (Langfeldt, Gleine and Estorff, Von, 2015), indicating that potential optimized elements can emerge for new applications.

Boundary-Element

This last proposed MAM module consists in the surrounding elements of a cell that impose boundary conditions to its surfaces or edges, thus altering its dynamic behavior. Initial MAMs had only a rigid frame as boundary-element for adequate membrane pre-stretching (Naify et al., 2010; Yang et al., 2008), whose stiffness already played a role in STL as seen in (Naify et al., 2012; Naify, et al., 2011). They stated that frame stiffness becomes an important factor as MAMs are scaled up to include multiple cells and experimented with its influence in a four-celled grid. Since the frame is an integral part of the MAM, its own vibrations alter the overall STL. Compliant frames promote a diminished STL peak and decrease its bandwidth by shifting the second mode to lower frequencies, as well as introducing its own resonance between both modes in the spectrum.

Although frame geometry is usually determined by membrane design, the opposite path is interesting due to the possibility of using off-the-shelf structures. Sui et al. (2015) and Lu et al. (2016) combined hexagonal honeycomb frames, known for their high stiffness/weight ratio, with elastic membranes to improve low frequency STL. Honeycomb structures were also studied in (Naify, Huang, et al., 2011), where they were associated with different gas layers for impedance mismatch and improved STL, and in (Tang et al., 2017), who used corrugated honeycomb cores associated with micro-perforations for broadband sound absorption. These last two, though membrane-less, can serve as potential boundary-elements for improving MAM acoustic performance.

Traditional sound attenuating constructions have also been employed as boundary-elements alongside MAMs, such as porous absorbers, largely used in acoustic treatment due to their good mid- to high-frequency absorption. These materials contain open pores that lead to thermal and viscous energy dissipation, which are effective only for significant particle velocities found distant from a rigid boundary condition (velocity equals zero). A large material thickness is then needed for better low-frequency absorption, which is often unfeasible (Cox and D'Antonio, 2017; Yang and Sheng, 2017). Thus, such materials could potentially benefit from a MAM coupling for broadband acoustic insulation and this combination is explored in (Wang et al., 2018), where two MAMs coupled with fiberglass wool as dissipative medium present coherent perfect absorption between 200-1000Hz.

Another commonly employed boundary-element is the Helmholtz resonator (HR), a classic sound absorbing device composed of an acoustic neck and cavity, representing an acoustic mass and compliance, respectively. Its resonant frequency can be calculated through:

$$\mathbf{f_0} = \frac{\mathbf{c}}{\mathbf{2\pi}}\sqrt{\frac{\mathbf{S}}{\mathbf{L\prime V}}} \tag{5}$$

where S and L' are the neck's area and effective length and V is the cavity's volume. In a HR's resonance, air vibrates rapidly in the neck region, inducing energy dissipation through thermoviscous losses.

Side-mounted HRs are commonly employed in duct noise control since there is little flow disturbance. Fu et al. (2017) improves this construction's performance by coupling the HRs with slightly detuned DMRs containing either a single mass or eccentric asymmetric masses like (Mei et al., 2012). Through asymmetric reflection and absorption, the first has shown an enhanced STL in the resonance region compared to single HRs, whereas the second exhibited improved multiple frequency STL not seen in sole HRs. Yang et al. (2015) also used a single mass DMR backed by a HR mounted laterally, but coupled it with another orthogonal single DMR and tuned them for degenerate resonances. Almost perfect absorption was obtained for wavelengths ten times lower than sample size.

Metasurfaces containing HRs for normal sound incidence are yet unexplored boundary-elements for MAM. Li et al. (2016) and Yamamoto (2018) developed metasurfaces with HRs which resulted in extraordinary absorption and enhanced STL respectively, but could still be coupled to DMRs as seen in side-mounted HRs for superior performance.

A last boundary-element that derives from traditional sound attenuating concepts are micro-perforated panels (MPPs), rigid plates containing periodically spaced holes with submillimeter dimensions that act as acoustic resistance with low acoustic mass reactance for energy dissipation. They were extensively studied by Maa (1998), who formulated the equations necessary for analyzing the perforation's role in sound absorption, which is mainly dependent of the maximum absorption coefficient, the resonance frequency and a perforate constant. These depend on geometric parameters such as hole diameter and cavity length. MPPs have already been combined with a reflecting surface to enhance energy density and thus sound absorption (Yang and Sheng, 2017), and with HRs to improve low-frequency performance (Park, 2013; Zhao, Yu and Wu, 2016), but never to DMRs, which can lead to great sound attenuation in broadband frequency.

INTEGRATED DESIGN METHOD

Fully coupled vibro-acoustic finite element models are used to illustrate the proposed approach to MAM design. A novel MAM is envisioned combining the STL potential of different modules in order to reduce overall transmission. Models for each module were constructed under similar physics and boundary conditions to ensure a consistent correlation and comparison between each numerical result. The resulting STL curve was then compared to the data obtained experimentally in an impedance tube setup, thus validating the computational model. The concepts were analyzed in a range until 2000 Hz due to the tube's upper limit.

Concerning model construction, a round waveguide with the structure under test is used to simulate the impedance tube condition and predict STL between the incident and outgoing sound pressure fields. Its diameter measures 72 mm to match the size of the experimental apparatus in which the sample is to be tested. The waveguide's length is 900mm at each side of the metastructure, where 800 mm of the posterior side is modelled as a Perfectly Matched Layer (PML) to simulate an anechoic termination after sound transmission. The waveguide surroundings are modelled as sound hard boundaries, except for the inlet surface, where a planar wave radiation condition with an incident pressure field of 1 Pa is set and the outlet surface after the PML, which is also modelled as a planar wave radiation boundary. Sound power is measured at the inlet port and the PML's interface with the outgoing pressure field by integrating the following equation over the waveguide's surface:

$$\mathbf{W_{i/o}} = \frac{|\mathbf{p_{i/o}}|^2}{\mathbf{2\rho c}} \tag{6}$$

where $W_{i/o}$ is the incoming/outgoing sound power, $p_{i/o}$ the incoming/outgoing sound pressure and ρ air density. STL is then calculated as:

$$\mathbf{STL} = \frac{\mathbf{W_i}}{\mathbf{W_o}} \tag{7}$$

The validation of the constructed numerical models is realized by comparing the numerical results to STL curves obtained in an acoustic plant composed of a two tube, four microphones setup, where the sample is held in the beginning of the second tube and is sealed with Vaseline. An anechoic and rigid termination are used in order to employ the two-load transmission loss method as post-processing, using the measured pressure transfer functions from the four microphones to calculate STL.

The integrated design procedure begins with the definition of the stiffness-element and an analysis of its sole STL performance. A circular membrane with 19.2 mm diameter and 0.19 mm thickness made of latex rubber is chosen based on the available testing conditions. The mechanical properties of the rubber have been determined by tensile testing and fed to the model. For a pre-stress of 1.9 MPa, they are defined as $E_{me} = 0.52\,MPa$, $\nu_{me} = 0.48$ and $\rho_{me} = 1050.35\,kg/m^3$. The aforementioned tension is applied as initial stress in both axis of the membrane's surface. The pre-stress causes membrane elongation, which by Poisson effect induces a reduction in the membrane's thickness that must be considered in order to represent its dynamics properly. In this case, the original membrane thickness is reduced to 0.06mm. As the impedance tube diameter is considerably larger than the membrane sample, this model should also considers the rigid frame that holds the membrane aligned with the waveguide, since it influences overall STL due to its binding to the mass law. The support is envisioned as a printed 10mm thick ABS plate, whose properties are defined as $E_{st} = 5\,GPa$, $\nu_{me} = 0.36$ and $\rho_{me} = 980\,kg/m^3$. An important remark is that this support plays a role in sound transmission, acting as a barrier in its corresponding area. An increase in STL is then expected, especially in higher frequencies as seen in the *mass-law*, which is not related to the MAM's resonant behaviour but can be attributed to a boundary-element factor. The both numerical and experimental resulting STL profiles are seen in Fig. 4 and characterizes a worsening performance with frequency increase until the membrane's first radiating mode near 1660 Hz, where a transmission maximum is present, followed by increasing STL after the resonance. Although STL is around 40 dB at 100 Hz, it decays significantly due to mode's effect and is under 25 dB over 1000 Hz, being insufficient to attenuate the noise produced by loud live music, for instance. Deviation between model and experiment consists in less than 2% in frequency and around 5dB in STL, which is acceptable since the impedance tube's error consists in circa 3dB.

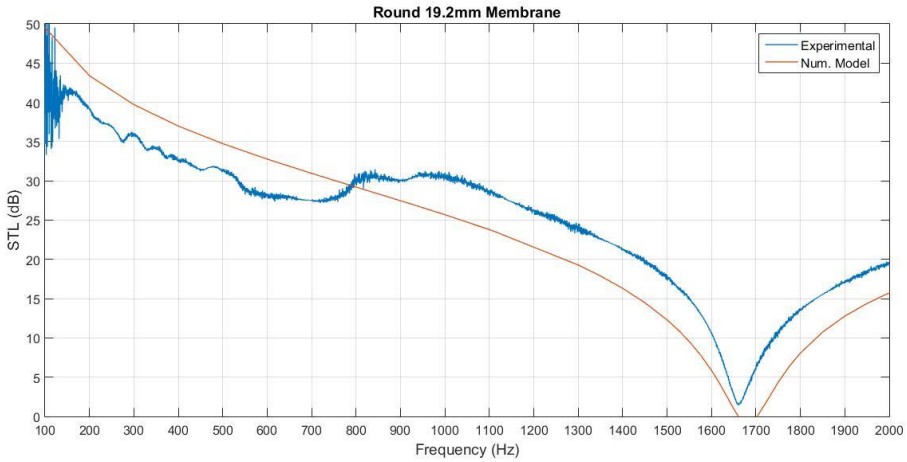

Figure 4 – Sound transmission loss from a sole 19.2mm diameter rubber membrane.

As seen in the previous section, the addition of a mass-element shifts the original membrane modes to lower-frequencies and introduces a high reflecting anti-resonance, which can be used to improve the performance of the sole stiffness-element. A circular central mass is then added to the membrane sample in order to enhance low frequency STL performance. Again due to experimental conditions, the modelled mass has a 5 mm diameter and 2 mm thickness and weights 0.33 g and its mechanical properties are defined as $E_{ma} = 200\ GPa$, $\nu_{ma} = 0.3$ and $\rho_{ma} = 8327\ kg/m^3$, considering both mass and the adhesive necessary for its binding.

The STL curve for the DMR obtained numerically was also compared with the impedance tube results and both are illustrated in Fig.5. Both setups show great coherence in the first vibrating mode and anti-resonance with almost no difference in terms of frequency. A large deviation is though seen at the peak STL value, which can be attributed to the lack of damping consideration in the model, since it is certainly present in the membrane dynamics. At higher frequencies, model and experiment still present similar results until around 1000 Hz, where the measured sample shows increasing STL with frequency whereas the model continues to decline. The seen STL increment corresponds to the *mass-law* of the frame overpowering the DMR's dynamic, which was not seen in the model because the frame's walls were modelled as soundhard to spare computational cost, thus neglecting its bending dynamics. In this configuration, the first radiating mode is then drawn to the lower frequency of 198 Hz, where a STL dip is followed by a peak caused by the hybridization between the two radiating modes. The STL performance is greatly improved after 230 Hz compared to the previous concept, as seen in Fig. 6, with a STL peak around 300 Hz of 48 dB, but is significantly worsened at lower frequencies dominated by the first radiating mode. STL also tends to diminish in the region dominated by the *mass-law* due to the DMR's second radiating mode, which causes another transmission maximum and tends to create another band where the sole membrane performance is superior after 2000 Hz.

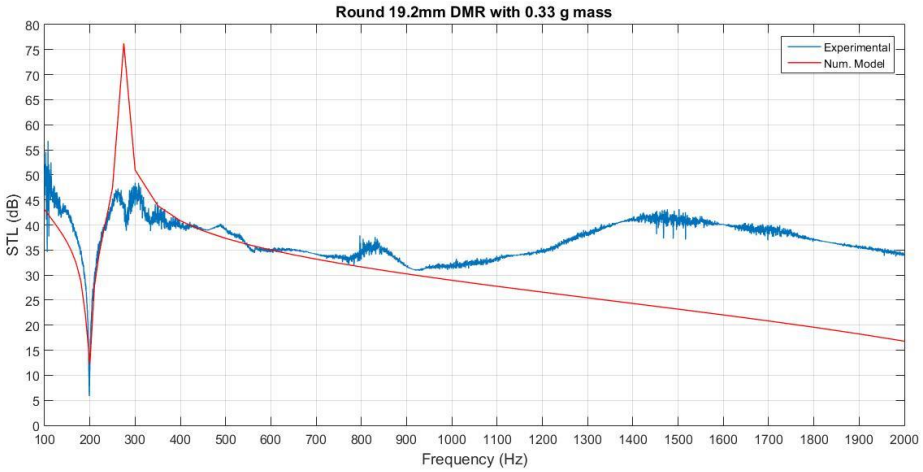

Figure 5 – Sound transmission loss from a 19.2mm diameter DMR with 0.33g mass.

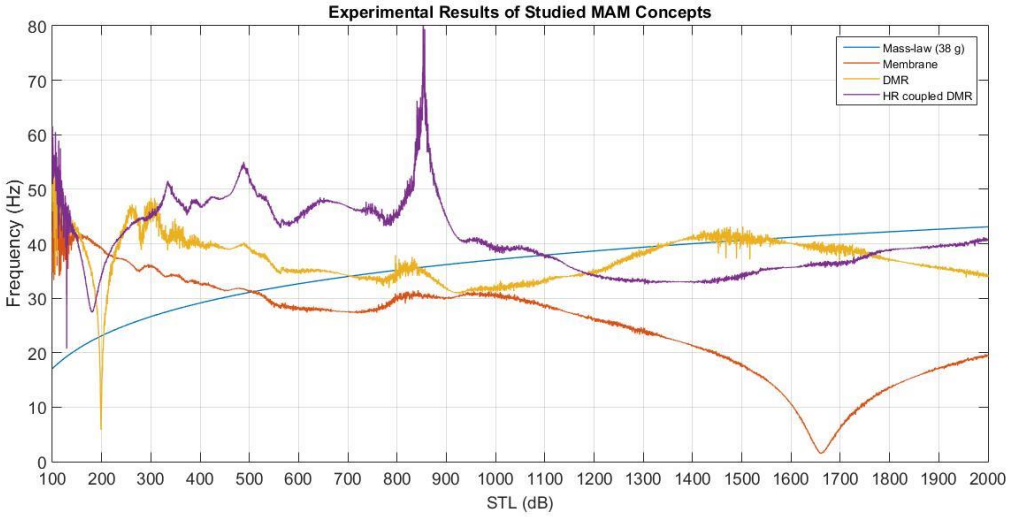

Figure 6 – Experimental STL curves of the different studied MAM concepts and equivalent *mass-law*.

It is then clear that, although this MAM concept is better than the sole membrane after the first resonance, it still needs improvement around the transmission maxima related to the DMR's resonances. A complementary boundary-element could then be designed to enhance STL in the two deficient regions, turning the determined frequency ranges into design

conditions for this element. As seen in literature such as (Yamamoto, 2018), metasurfaces containing HRs can be tuned to a determined frequency for improved STL at its resonance whilst still having increased STL with frequency due to the *mass-law*. Therefore, a HR metasurface tuned near the first resonance from the previous MAM construction appeals as an interesting boundary-element for broadening STL performance.

A metasurface with an embedded HR backed by a traditional DMR is then proposed as shown in Fig. 7, and is made of the same material as the previous support. The HR has a neck length of 10 mm, a neck diameter of 1.4 mm and a cylindrical cavity volume of 4398 mm³, determined by Eq. (5) to induce a resonance near 330 Hz, circa 100 Hz higher than the DMR's first radiating mode frequency. Though a perfectly matched Helmholtz resonance to the DMR's first mode was desired, it was not possible due to manufacturing issues. The resulting STL profile is displayed in Fig. 7, where a partial improvement compared to the previous design is observed. The Helmholtz resonance affects the first mode by shifting it to 180 Hz and greatly improving the STL minimum, which previously was 5 dB and was elevated to 28 dB due to the STL peak at 334 Hz of the HR. At higher frequencies, the HR structure's *mass-law* takes over the second DMR resonance, avoiding a worsening performance after 1770 Hz. However, between 1200-1700 Hz the original DMR still presents better performance, between the *mass-law* action and the point where the second resonance begins to influence its performance. The resulting STL curve is also compared to a numerical solution in Fig. 8, but aside from the first resonance did not present great coherence. As in the previous case, the simulation failed to capture the full effect of the frame in STL at higher frequencies, which is a necessary revision for future work. Also surprising is the large peak observed at 850 Hz, completely unpredicted and not seen in the simulation results. Its existence is not due to the MAM dynamics, but probably caused by the formation of standing waves in the tube badly captured by the microphone positions. It shall then be ignored since it does not really represent the material's behaviour.

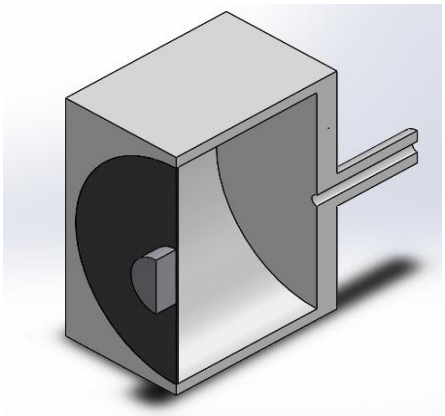

Figure 7 – Isometric view from a lateral section of the proposed combination of DMR and HR

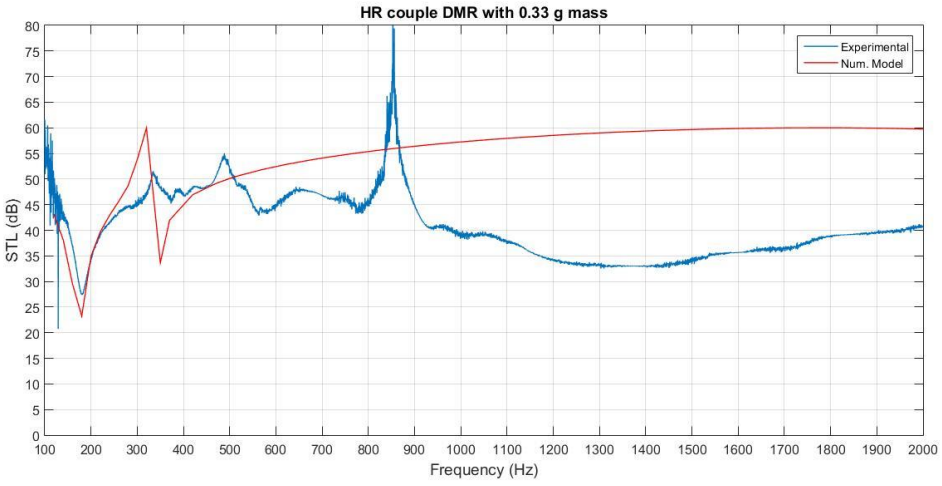

Figure 8 – Sound transmission loss of a HR coupled DMR.

Another important consideration is the relationship between each concept's mass and STL potential. The sole membrane resonator estimated weight is approximately 0.018 g and the DMR's is around 0.345 g. The frame accounts for the larger weight in these two, since it weights circa 36 g, whereas the frame with the imbued HR weights around 38g. All three studied concepts are compared to an equivalent barrier of 38g that follows the *mass-law* from Eq. (1) in Fig. 6 and are seen to have a better STL potential in different frequency bands. The membrane only MAM shows a better performance until 500 Hz, the DMR until 700 Hz except for the resonance caused dip and the HR coupled DMR until 1100 Hz. The latter also tends to match the prediction of the *mass-law* curve after 2000 Hz. Although this solely could

justify the use of this novel MAM concept as a smarter weight distribution for an acoustic solution, its added frame weight (2 g) is still several times the one of a single DMR or membrane resonator. This brings up the question if one should utilize the proposed boundary-element or employ the mass-equivalent number of DMRs or membranes tuned in different frequencies for a better STL result.

A positive aspect of the proposed MAM is its robustness at higher frequencies due to the partial binding to the mass-law, whereas multiple resonators would still exhibit multiple STL dips in their resonances as seen in (Naify et al., 2012), resulting in worse performance around these frequencies. However, in their anti-resonances, the STL peaks tend to surpass significantly the proposed MAM's STL profile, which may be more interesting depending on the application.

CONCLUSIONS

An integrated design approach to metamaterial design was proposed, dividing a MAM cell into three basic units: a mass-, a stiffness- and a boundary-element. The fundamentals and possibilities from each module were thoroughly described through concepts found in recent works in the field of acoustic metamaterials. It has been stated that the resonant properties of the final MAM respect the dynamic behavior of the respective constituents, and this can be used in order to improve MAM performance in terms of shaping the STL profile for broadband attenuation and preventing transmission maxima.

Using the possible elements described for each module, a novel MAM concept was envisioned to exemplify this sequential design procedure of modular construction. With a latex rubber membrane as basis, it was seen how the STL curve was altered with the addition of a rigid disk as mass-element and a HR as boundary-element. The mass-element transposed the former membrane radiating mode to a much lower frequency and introduced a strong anti-resonance, thus altering directly the membrane's dynamic behavior. The boundary-element was thought and tuned to complement the previous construction's deficient regions and when coupled was able to improve the desired weaknesses. It can then be concluded that an integrated design, that is: designing a MAM cell considering the particular resonances of its elements and then coupling them is valid, since they influence the resulting STL profile in the tuned frequencies. The HR coupled DMR showed significant improvement in terms of better sound attenuation in terms of value and band, but also raised the questioning of how the STL performance relates to cell weight. It is necessary not only to compare a new design to the equivalent *mass law*, but also with different assemblies of the resonant elements, which can prove advantageous according to the application.

In order to fully comprehend the phenomena involving the proposed design and clarify even further the problem of MAM design, the present research find itself in an ongoing campaign to refine simulation results in order to avoid discordances due to modeling assumption concerning frame modelling. It also aims at upgrading the quality of its experimental apparatus, so that false unwanted peaks become absent in future measures. Future work also involves extending this research to multi-celled structures and study how periodicity can influence in overall performance.

ACKNOWNLEDGMENTS

The authors acknowledge the São Paulo State Reseach Foundation – FAPESP, under grant #2018/05793-2 for the financial support.

REFERENCES

Blevins, M. G.,Lau, S.-K.,Wang, L. M., 2016, "Design and optimization of membrane-type acoustic metamaterials using genetic algorithms", The Journal of the Acoustical Society of America, Vol. 140, No. 4, p. 3431.

Chen, Y. et al., 2014, "Analytical coupled vibroacoustic modeling of membrane-type acoustic metamaterials: Plate model", The Journal of the Acoustical Society of America, Vol. 136, No. 6, pp. 2926–2934.

Cox, T. J.,D'Antonio, P., 2017, Acoustic Absorbers and Diffusers.

Cummer, S. A.,Christensen, J.,Alù, A., 2016, "Controlling sound with acoustic metamaterials", Nature Reviews Materials, Vol. 1, No. 16001, pp. 1–14.

Cummer, S. A.,Schurig, D., 2007, "One path to acoustic cloaking", New Journal of Physics, Vol. 9.

Fleury, R. et al., 2015, "Nonreciprocal Acoustics", Acoustics Today, Vol. 11, No. 3, pp. 14.

Fu, C. et al., 2017, "Hybrid membrane resonators for multiple frequency asymmetric absorption and reflection in large waveguide", Applied Physics Letters, Vol. 110, No. 2.

Huang, C.-C., 2000, "Overview of modular product development", Proceedings of the National Science Council Republic of China Part A Physical Science and Engineering, Vol. 24, No. 3, pp. 149–165.

Huang, T.-Y.,Shen, C.,Jing, Y., 2016, "Membrane- and plate-type acoustic metamaterials", The Journal of the Acoustical Society of America, Vol. 139, No. 6, pp. 3240–3250.

Klironomos, A. D.,Economou, E. N., 1998, "Elastic wave band gaps and single scattering", Vol. 105, No. 5, pp. 327–332.

Kushwaha, M. S. et al., 1993, "Acoustic Band Structure of Periodic Elastic Composites", Vol. 71, No. 13, pp. 2022–2025.

Langfeldt, F. et al., 2017, "Perforated membrane-type acoustic metamaterials", Physics Letters, Section A: General, Atomic and Solid State Physics, Vol. 381, No. 16, pp. 1457–1462.

Langfeldt, F.,Gleine, W.,von Estorff, O., 2015, "Analytical model for low-frequency transmission loss calculation of membranes loaded with arbitrarily shaped masses", Journal of Sound and Vibration, Vol. 349, pp. 315–329.

Li, J. et al., 2016, "A sound absorbing metasurface with coupled resonators", Applied Physics Letters, Vol. 109, No. 9, pp. 3–6.

Liu, Z. et al., 2000, "Locally Resonant Sonic Materials", Science, Vol. 289, No. 5485, pp. 1734–1736.

London, A., 1949, "Transmission of Reverberant Sound Through Single Walls", Journal of Research of the National Bureau of Standards, Vol. 42.

Lu, K. et al., 2016, "A lightweight low-frequency sound insulation membrane-type acoustic metamaterial", AIP Advances, Vol. 6, No. 2.

Maa, D.-Y., 1998, "Potential of microperforated panel absorber", The Journal of the Acoustical Society of America, Vol. 104, No. 5, pp. 2861–2866.

Mei, J. et al., 2012, "Dark acoustic metamaterials as super absorbers for low-frequency sound", Nature Communications, Vol. 3, pp. 756–757.

Möser, M., 2009, Technische Akustik.

Naify, C. J. et al, 2010, "Transmission loss and dynamic response of membrane-type locally resonant acoustic metamaterials", Journal of Applied Physics, Vol. 108, No. 11.

Naify, C. J.,Chang, C. M.,McKnight, G.,Nutt, S., 2011, "Transmission loss of membrane-type acoustic metamaterials with coaxial ring masses", Journal of Applied Physics, Vol. 110, No. 12.

Naify, C. J.,Chang, C. M.,McKnight, G.,Scheulen, F.,et al, 2011, "Membrane-type metamaterials: Transmission loss of multi-celled arrays", Journal of Applied Physics, Vol. 109, No. 10.

Naify, C. J.,Huang, C.,et al., 2011, "Transmission loss of honeycomb sandwich structures with attached gas layers", Applied Acoustics, Vol. 72, No. 2–3, pp. 71–77.

Naify, C. J. et al., 2012, "Scaling of membrane-type locally resonant acoustic metamaterial arrays", The Journal of the Acoustical Society of America, Vol. 132, No. 4, pp. 2784–2792.

Park, S. H., 2013, "Acoustic properties of micro-perforated panel absorbers backed by Helmholtz resonators for the improvement of low-frequency sound absorption", Journal of Sound and Vibration, Vol. 332, No. 20, pp. 4895–4911.

Sui, N. et al., 2015, "A lightweight yet sound-proof honeycomb acoustic metamaterial", Applied Physics Letters, Vol. 106, No. 17, pp. 1–5.

Tang, Y. et al., 2017, "Hybrid acoustic metamaterial as super absorber for broadband low-frequency sound", Scientific Reports, Vol. 7, No. July 2016, pp. 1–11.

Wang, X. et al., 2018, "Acoustic perfect absorption and broadband insulation achieved by double-zero metamaterials", Applied Physics Letters, Vol. 112, No. 2.

Yamamoto, T., 2018, "Acoustic metamaterial plate embedded with Helmholtz resonators for extraordinary sound transmission loss", Journal of Applied Physics, Vol. 123, No. 21.

Yang, M. et al., 2013, "Coupled membranes with doubly negative mass density and bulk modulus", Physical Review Letters, Vol. 110, No. 13, pp. 1–5.

Yang, M.,Li, Y.,et al., 2015, "Sound absorption by subwavelength membrane structures: A geometric perspective", Comptes Rendus - Mecanique, Vol. 343, No. 12, pp. 635–644.

Yang, M.,Ma, G.,et al., 2015, "Subwavelength perfect acoustic absorption in membrane-type metamaterials : a geometric perspective ", No. April 2016.

Yang, M.,Sheng, P., 2017., "Sound Absorption Structures: From Porous Media to Acoustic Metamaterials", Annual Review of Materials Research, Vol. 47, No. 1, pp. 83–114.

Yang, Z. et al., 2008, "Membrane-type acoustic metamaterial with negative dynamic mass". Physical Review Letters, Vol. 101, No. 20, pp. 1–4.

Zhang, Y. et al., 2012, "Theoretical investigation of the sound attenuation of membrane-type acoustic metamaterials", Physics Letters, Section A: General, Atomic and Solid State Physics, Vol. 376, No. 17, pp. 1489–1494.

Zhao, X. D.,Yu, Y. J.,Wu, Y. J., 2016, "Improving low-frequency sound absorption of micro-perforated panel absorbers by using mechanical impedance plate combined with Helmholtz resonators", Applied Acoustics, Vol. 114, pp. 92–98.

RESPONSIBILITY NOTICE

The author(s) is (are) the only responsible for the printed material included in this paper.